Weierstraß-Institut

für Angewandte Analysis und Stochastik

im Forschungsverbund Berlin e. V.

Preprint ISSN 0946 – 8633

The role of reactive reaction intermediates in two-step heterogeneous electrocatalytic reactions: A model study

J. Fuhrmann[1], H. Zhao[1], H. Langmach[1], Y.E. Seidel [2], Z. Jusys[2],

R. J. Behm[2]

submitted: July 8, 2010

[1] Weierstrass Institute for Applied Analysis and Stochastics, Mohrenstr. 39, 10117 Berlin, Germany

[2] Institute of Surface Chemistry and Catalysis, Ulm University, 89069 Ulm, Germany

No. 1522

Berlin 2010

2010 *Mathematics Subject Classification.* 35K20, 65N99.

Key words and phrases. Finite volume method, electrocatalysis.

Edited by
Weierstraß-Institut für Angewandte Analysis und Stochastik (WIAS)
Mohrenstraße 39
10117 Berlin
Germany

Fax: +49 30 2044975
E-Mail: preprint@wias-berlin.de
World Wide Web: http://www.wias-berlin.de/

Abstract

Experimental investigations of heterogeneous electrocatalytic reactions have been performed in flow cells which provide an environment with controlled parameters. Measurements of the oxygen reduction reaction in a flow cell with an electrode consisting of an array of Pt nanodisks on a glassy carbon substrate exhibited a decreasing fraction of the intermediate H2O2 in the overall reaction products with increasing density of the nanodisks. A similar result is true for the dependence on the catalyst loading in the case of a supported Pt/C catalyst thin-film electrode, where the fraction of the intermediate decreases with increasing catalyst loading. Similar effects have been detected for the methanol oxidation. We present a model of multistep heterogeneous electrocatalytic oxidation and reduction reactions based on an adsorption-reaction-desorption scheme using the Langmuir assumption and macroscopic transport equations. A continuum based model problem in a vertical cross section of a rectangular flow cell is proposed in order to explain basic principles of the experimental situation. It includes three model species A, B, C, which undergo adsorption and desorption at a catalyst surface, as well as adsorbate reactions from A to B to C. These surface reactions are coupled with diffusion and advection in the Hagen Poiseuille flow in the flow chamber of the cell. High velocity asymptotic theory and a finite volume numerical method are used to obtain approximate solutions to the model. Both approaches show a behavior similar to the experimentally observed. Working in more general situations, the finite volume scheme was applied to a catalyst layer consisting of a number of small catalytically active areas corresponding to nanodisks. Good qualitative agreement with the experimental findings is established for this case as well.

1 Introduction

Heterogeneous electrocatalytic oxidation and reduction reactions can be modeled by an adsorption-reaction-desorption scheme based on the Langmuir model for adsorption /desorption, see e.g. [1, 2, 3, 4]. If the adsorbate reaction involves multiple reaction steps of the type $A \rightarrow B \rightarrow C$, desorption, re-adsorption and further conversion of reactive intermediates B can occur [7]. Although such a sequence was proposed to severely affect not only the reaction activity, but in particular the reaction selectivity (product yield) [7], they have not been considered in model descriptions of electrocatalytic reactions so far [5]. This is the topic of the present paper, where we introduce a model description based on macroscale partial differential equations describing the coupling between transport and reaction, which attempts to explain this experimental situation. Asymptotic theory and, alternatively, the finite volume numerical method are used in order to obtain approximate solutions of the resulting model. Experimentally, reactions of this kind have been investigated in different types of flow cell measurements, which allow a precise control of the reaction and transport parameters. Specifically, the present work refers to recent findings on the correlation between product distribution in the oxygen reduction reaction and the density of Pt ultra-microelectrodes on nanostructured Pt/GC model electrodes or the electrolyte flow [6,7]. The model electrodes consist of arrays of catalytically active Pt nanodisks of defined size (diameter ~ 100 nm) and separation on an electrochemically inert planar glassy carbon (GC) substrate, which are fabricated by hole-mask colloidal lithography (HCL) [8]; the electrocatalytic measurements were performed in a double disk dual thin-layer flow cell [9], which allows for the simultaneous detection of Faradaic current and product distribution (formation of H_2O and H_2O_2). These measurements exhibited a clear correlation between the product distribution and the density of the Pt ultra-microelectrodes, with the relative amount of reaction intermediates in the overall reaction products decreasing with increasing density of catalytically active Pt nanodisks [6, 7]. Similar trends have been reported for the oxidation of formaldehyde [10] and methanol [11] on these nanostructured Pt/GC electrodes. The same is true for the dependency of the product yields on the catalyst loading in the case of a single large Pt/C electrode, e.g., for the electro-oxidation of methanol [12]. A 'desorption – re-adsorption – reaction' process has been postulated to be responsible for this effect [7].

The complex nature of interactions between transport and heterogeneous reaction kinetics triggered several groups to consider model studies of nanodisk arrays in order to improve the understanding of the occurring effects. Liu et al [13] regard active spots of a size of 10nm and less where the electroneutrality assumption – which is behind the model presented in this paper – can not anymore replace the Poisson equation. They focus on the influence of the potential and use a refined model beyond the classical Butler Volmer like ansatz. They conclude that with decreasing size of a nanodisk, the relative strength of these effects increases. Wang et al [14] focus on a model describing the effect of adsorbate spillover in hydrogen evolution caused by surface diffusion of adsorbed hydrogen from the catalytically active area to the support material.

Our model approach focuses on adsorption, desorption, adsorbate reaction, re-adsorption and further conversion of the reaction intermediate at fixed temperature and fixed applied potential. Using the Arrhenius and Butler-Volmer relations, these restrictions could be removed. Another possible improvement would be the introduction of surface diffusion of adsorbed species. We stick to the simpler problem as we believe that it eases the explanation of the observed effects. Different from the qualitative proposals in refs. [6] and [7], the model description will be based on macroscopic concepts like mean field theory and Fick's diffusion characteristics.

The model problem and main experimental trends are introduced in section 2. Section 3 is devoted to numerical results which show that the trends resulting from these model calculations are qualitatively similar to those found experimentally. Namely, the proportion of the intermediate decreases with increasing catalyst loading, or with increasing density of catalytically active areas (e.g. nanodisks), henceforth called active areas. In section 4, asymptotic expansions for large flow velocities are derived. Using these expressions, in section 5, the results from the numerical investigation are confirmed for the case of large velocities. Section 6 concludes the paper.

2 A thin layer flow cell model for consecutive reactions at constant temperature and potential

2.1 Description of the model

The mathematical model is established in a two-dimensional vertical cross section through a rectangular flow cell. In the mathematical model, this cross section coincides with a rectangular domain Ω with boundary Γ. This boundary is further subdivided into functional sections. At fixed temperature T and fixed pressure p, an electrolyte containing dissolved species A enters the cell at the inlet (boundary section Γ_{in}), flows over the working electrode, and leaves the cell at the outlet (boundary section Γ_{out}). At the inlet, the concentration of A is given by c_{A0}. The species are transported by both convection in the velocity field of the electrolyte parallel to the x-axis, and by diffusion through the two-dimensional reactor and to the electrode (see Fig. 1). At the electrode, they can adsorb on the catalytically active areas (number of active areas: n_{act}, length of an active area: l_{act}, boundary section: Γ_{cat}) and react to the reaction intermediate B with a given probability. In the model, we allow the intermediate B to either desorb or to react to the final product C with given probabilities. Desorbed B is allowed to re-adsorb again or will be transported to the outlet and leave the cell together with non-converted A and the newly formed final product C. Re-adsorbed B will again either react to C or desorb anew. Adsorption of A or B is only possible on free catalyst sites.

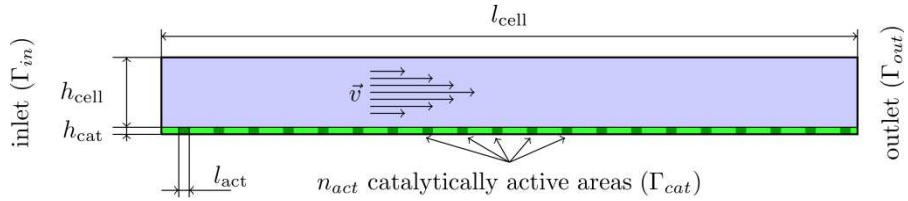

Figure 1: Cross section through the hypothetical flow cell.

For sufficiently high ion concentration of the carrier electrolyte, ohmic potential drops are negligible. Furthermore, the simple rectangular channel geometry allows to use a fixed velocity field given by an analytical expression. As in [15], we neglect electrical effects and transport effects of protons and electrons.

Assuming a given potential and a given temperature, the proposed reaction mechanism, together with the rate expressions due to Langmuir assumption and mass action law at the flow cell electrode reads as follows:

$$A + s \quad \overset{k_A^{\pm}}{\rightleftharpoons} \quad A_{\text{ads}}\,, \qquad r_A = \hat{k}_A^{+} c_A \theta_f - k_A^{-} \theta_A \tag{1}$$

$$A_{\text{ads}} \quad \overset{k_{AB}^{\pm}}{\rightleftharpoons} \quad B_{\text{ads}}\,, \qquad r_{AB} = k_{AB}^{+} \theta_A - k_{AB}^{-} \theta_B \tag{2}$$

$$B + s \quad \overset{k_B^{\pm}}{\rightleftharpoons} \quad B_{\text{ads}}\,, \qquad r_B = \hat{k}_B^{+} c_B \theta_f - k_B^{-} \theta_B \tag{3}$$

$$B_{\text{ads}} \quad \overset{k_{BC}^{\pm}}{\rightleftharpoons} \quad C_{\text{ads}}\,, \qquad r_{BC} = k_{BC}^{+} \theta_B - k_{BC}^{-} \theta_C \tag{4}$$

$$C + s \quad \overset{k_C^{\pm}}{\rightleftharpoons} \quad C_{\text{ads}}\,, \qquad r_C = \hat{k}_C^{+} c_C \theta_f - k_C^{-} \theta_C \tag{5}$$

$$1 = \theta_f + \theta_A + \theta_B + \theta_C \tag{6}$$

where $\hat{k}_X^{+} = \frac{k_X^{+}}{c_{\text{ref}}}$ for $X = A, B, C$. k_X^{+} and k_X^{-} are the reaction coefficients, c_{ref} is the reference concentration, c_A, c_B, and c_C are the concentration of species A, B and C, θ_A, θ_B and θ_C are the coverages of the adsorbed species (fractions of catalyst sites occupied by these species), and $\theta_f = 1 - \theta_A - \theta_B - \theta_C$ describes the coverage of the remaining free catalyst sites.

Reaction (1) describes the adsorption of species A on a free site s. Reaction (2) we can imagine as a surface reaction which produces B. Step (3) is an adsorption - desorption reaction of the intermediate B on another free site s, which in many models (e.g., [5]) has not been included so far. A second surface reaction (4), (5) may transfer the intermediate B into the final product C. Finally, equation (6) describes the balance of free and occupied catalyst sites. We assume a fixed applied potential, and a fixed temperature. This assumption will allow us to model the reaction terms using a straightforward *ansatz* based on the law of mass action.

The transport of each of the species $X = A, B, C$ is described by the convection diffusion equation

$$\partial_t c_X - \nabla \cdot (D_X \nabla c_X - c_X \vec{v}) = 0 \tag{7}$$

D_X are molecular diffusion coefficients, and $\vec{v}$ is the fluid velocity.

As boundary conditions at the inlet we assume a given precursor concentration and zero concentrations of the intermediate and the product:

$$c_A|_{\Gamma_{\text{in}}} = c_{A0} = 1, c_B|_{\Gamma_{\text{in}}} = 0, c_C|_{\Gamma_{\text{in}}} = 0.$$

At the outlet, we assume outflow boundary conditions [16] for $X = A, B, C$:

$$(D_X \nabla c_X - c_X \vec{v}) \cdot \vec{n} = -c_X \vec{v} \cdot \vec{n}.$$

At the electrode, we assume coupled surface reactions

$$\nabla \cdot (D_X \nabla c_X - c_X \vec{v}) = R_X = c_{\text{cat}} r_X, \tag{8}$$

where c_{cat} is the superficial density of available catalyst sites.

The system is closed by the rate equations for the adsorbed species, which are defined at the electrode surface:

$$\partial_t \theta_A = r_A - r_{AB} \tag{9}$$
$$\partial_t \theta_B = r_B + r_{AB} - r_{BC} \tag{10}$$
$$\partial_t \theta_C = r_C + r_{BC} \tag{11}$$

At all other sections of the boundary, we assume no mass transport through the boundary:

$$(D_X \nabla c_X - c_X \vec{v}) \cdot \vec{n} = 0.$$

We will restrict our considerations to the two-dimensional stationary case and assume a time independent velocity field. As, furthermore, the boundary conditions do not change in time, it is sufficient to obtain a stationary solution of the system (7), (9)-(11).

Due to the simple channel geometry of the flow cell, the velocity profile $\vec{v}$ can be assumed to follow the Hagen Poisseuille law

$$v_x = 4 \frac{y}{h_{\text{cell}}} \left(1 - \frac{y}{h_{\text{cell}}}\right) v_{\max}$$
$$v_y = 0$$

As a further consequence, in this case the evolution equations (9)-(11) turn into algebraic equations. Table 1 gives an overview over the values of the model problem parameters chosen for the further investigations. We assume all parameters as non-dimensionalized. The reaction constants have been chosen in order to demonstrate a certain possible qualitative behavior of the system. Therefore all forward reaction constants in the chain

$$A + s \rightleftharpoons A_{\text{ads}} \rightleftharpoons B_{\text{ads}} \rightleftharpoons C_{\text{ads}} \rightleftharpoons C + s$$

take the same large value, and all backward reaction constants of this chain take the same small value. The large value is also assigned to both backward and forward reaction constants of the reaction $B_{\text{ads}} \rightleftharpoons B + s$. We define the amounts of species X entering resp. leaving the flow cell per unit of time by

$$X_{\text{in}} = \int_{\Gamma_{\text{in}}} c_X \vec{v} \cdot \vec{n} \, ds, \quad X_{\text{out}} = \int_{\Gamma_{\text{out}}} c_X \vec{v} \cdot \vec{n} \, ds,$$

and the concentration of species X leaving the flow cell

$$c_{X,\text{out}} = \frac{\int_{\Gamma_\text{out}} c_X \vec{v} \cdot \vec{n}\ ds}{\int_{\Gamma_\text{out}} \vec{v} \cdot \vec{n}\ ds}.$$

Especially, we will be interested in the relative amount of reaction intermediates $\frac{B_\text{out}}{B_\text{out}+C_\text{out}}$ in the final products leaving the cell.

2.2 Main experimental trends

The main results of previous experimental studies on the influence of active particle density and electrolyte flow on the yield (relative amount) of the reactive reaction intermediate H_2O_2 in the oxygen reduction reaction [7] are summarized in the two plots shown in figure 2.

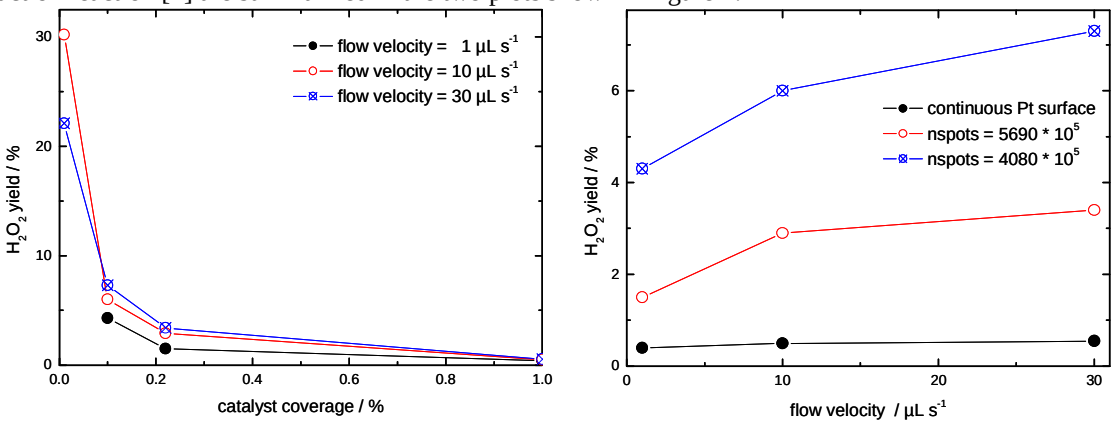

Figure 2: Fraction of the oxygen reduction reaction intermediate H_2O_2 measured at the reaction cell outlet as experimentally determined in [7] at a potential of 0.3 V. Left: Results obtained for different fixed electrolyte flow velocities (1 µL s^{-1}: line with filled circles, 10 µL s^{-1}: line with unfilled circles and 30 µL s^{-1}: line with crosses). Right: Influence of the electrolyte flow velocity at different coverages of Pt nanodisks (100 % Pt coverage – line with filled circles, 20 % Pt coverage – line with unfilled circles and 10 % Pt coverage – line with crosses).

The left panel shows the decrease of the H_2O_2 yield with increasing coverage of active Pt nanodisks on the planar glassy carbon substrate at different electrolyte flow rates, while the right panel illustrates the increase of the H_2O_2 yield with increasing electrolyte flow rate for two different densities of similarly sized Pt nanodisks and a fully Pt covered electrode, equivalent to a polycrystalline Pt electrode.

These findings have been obtained using a radial thin layer flow cell. They could be explained on a semi-qualitative scale accounting for 'desorption – re-adsorption – (further) reaction' of the intermediate (H_2O_2), where the probability for further conversion of hydrogen peroxide to water depends on the density of the active sites per geometric area (more efficient conversion towards the final product at higher density), and the electrolyte flow rate (thinner diffusion layer at higher flow rates) [6,7].

3 Numerical results

The model has been discretized by a Voronoi box based finite volume method as described and verified in [15,16]. Due to the current state of the numerical code, it was not possible to model the surface reactions directly. Instead, we replaced the electrode surface by a thin active reaction layer where we couple transport and reactions in the volume assuming zero velocity and high diffusion:

$$\begin{aligned}
\partial_t c_A - \nabla \cdot (D_A \nabla c_A - c_A \vec{v}) &= -R_A &&= -c_\text{cat}^\text{eff}\, r_A \\
\partial_t c_B - \nabla \cdot (D_B \nabla c_B - c_B \vec{v}) &= -R_B &&= -c_\text{cat}^\text{eff}\, r_B \\
\partial_t c_C - \nabla \cdot (D_C \nabla c_C - c_C \vec{v}) &= -R_C &&= -c_\text{cat}^\text{eff}\, r_C
\end{aligned}$$

where $c_\text{cat}^\text{eff} = c_\text{cat}/h_\text{cat}$, h_cat is the thickness of the catalyst layer. Correspondingly, equations (9)-(11) are assumed to be valid in this layer as well.

Table 1: Parameters and constants used in the numerical experiments

			Geometrical data
l_{cell}	=	128	cell length (in *x*-direction)
l_{act}	=	1,…,128	length (diameter) of a single catalytically active area (in *x*-direction)
n_{act}	=	1,…,64	number of catalytically active areas (in *x*-direction)
h_{cell}	=	1	cell height (in *y*-direction)
h_{cat}	=	10^{-10}	height of catalytically active areas (in *y*-direction)
			Reaction data
$v_{\max}$	=	1,…,500	max. velocity; default: 10
$c_{\text{cat}}^{\text{eff}}$	=	10,…,10^6	effective amount of catalyst sites per unit volume; default value: 10^5
c_{A0}	=	1	concentration (of *A*) at the inlet
D^{cell}	=	1	diffusivity of *A*, *B*, *C* within the cell region; default value: 1
D^{cat}	=	1	diffusivity of *A*, *B*, *C* within the catalyst region; default value: 1
k_A^+	=	10^5	reaction constant in (1)
k_A^-	=	10^{-5}	reaction constant in (1)
k_{AB}^+	=	10^5	reaction constant in (2)
k_{AB}^-	=	10^{-5}	reaction constant in (2)
k_B^+	=	10^5	reaction constant in (3)
k_B^-	=	10^5	reaction constant in (3)
k_{BC}^+	=	10^5	reaction constant in (4)
k_{BC}^-	=	10^{-5}	reaction constant in (4)
k_C^+	=	10^{-5}	reaction constant in (5)
k_C^-	=	10^5	reaction constant in (5)
			Derived data
L_{cat}	=	$n_{\text{act}} \cdot l_{\text{act}}$	total length of the catalyst region,
c_{cat}	=	$c_{\text{cat}}^{\text{eff}} \cdot h_{\text{cat}}$	superficial density of catalyst sites
N_{cat}	=	$c_{\text{cat}} \cdot L_{\text{cat}}$	total amount of catalyst

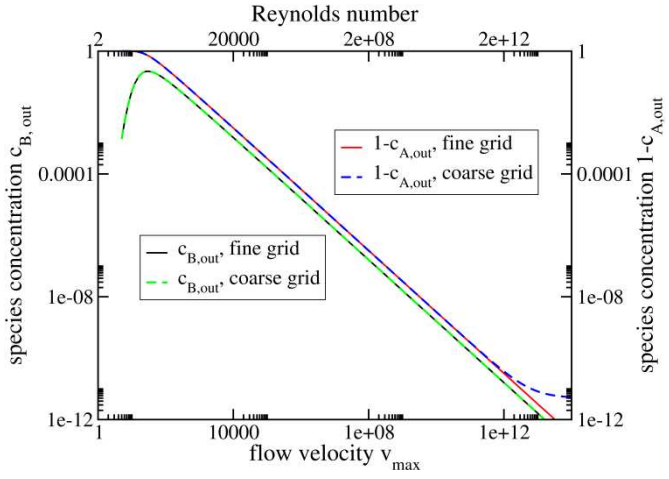

Figure 3: Outlet concentrations for different reacting species for large flow velocities on two different simulation grids

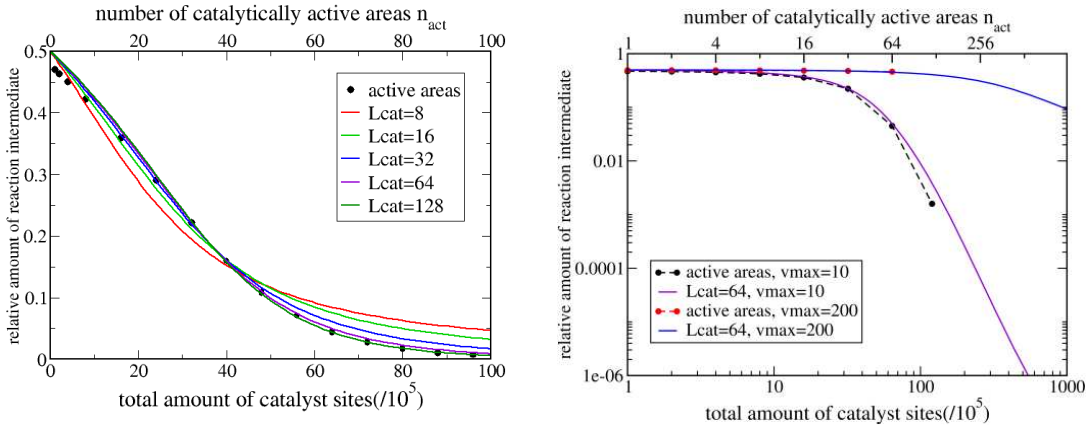

Figure 4: Relative amount of reaction intermediates $B_{\text{out}}/(B_{\text{out}} + C_{\text{out}})$ depending on the total amount of catalyst N_{cat}. Left: Results for fixed velocity and varying amounts of catalyst. Right: Influence of the flow velocity. Solid lines correspond to a single catalytically active area of length $L_{\text{cat}} = l_{\text{act}}$ and varying $c_{\text{cat}}^{\text{eff}}$. Dotted lines correspond to the variation of the number of equally sized catalytically active areas n_{act} of length $l_{\text{act}} = 1$ while keeping $c_{\text{cat}}^{\text{eff}}$ constant.

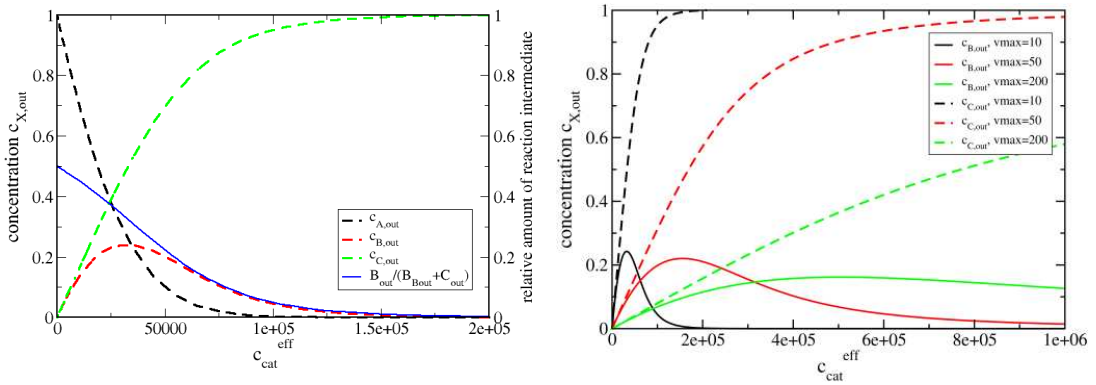

Figure 5: Left: Concentration of the respective species and relative amount of reaction intermediates at outlet depending on c_{cat} for $l_{\text{act}} = 1$ and $n_{\text{act}} = 64$ at $v_{\text{max}} = 10$. Right: Influence of the flow velocity on the species concentration.

3.1 Convergence of the method

Figure 3 is provided for verification purposes and demonstrates the ability of the numerical method to resolve the electrode boundary layer in such a way that grid convergence for the concentrations measured at the outlet is reached. We note a divergence of fine and coarse grid results for Reynolds numbers far beyond the transition to turbulent flow. Therefore we can assume sufficient accuracy of the discretization in the relevant velocity range.

3.2 Variation of the total amount of catalyst and the number of catalytically active areas

For a given number of catalytically active areas n_{act} of length l_{act} , the total length of the catalyst region, L_{cat}, is denoted by $L_{\text{cat}} = n_{\text{act}} \cdot l_{\text{act}}$, and the total amount of catalyst can be expressed as $N_{\text{cat}} = c_{\text{cat}} \cdot L_{\text{cat}}$.

Figure 4 shows the influence of N_{cat} on the relative amount of reaction intermediates $B_{\text{out}}/(B_{\text{out}} + C_{\text{out}})$ for varying numbers of catalytically active areas of fixed size l_{act}, keeping the superficial catalyst density c_{cat} (i.e. the amount of catalyst sites per unit surface area) in the catalytically active areas constant (dotted lines) and varying the superficial catalyst density for a single catalytically active area

with different length (lines without dots). Figure 5 shows this effect for one particular arrangement of catalytically active areas while varying the catalyst superficial density c_{cat}.

The results in figures 4 and 5 illustrate that the model reflects the experimental findings which show a decrease of the relative amount of H_2O_2 formation (reaction intermediate) with increasing amount of catalyst or number of nanodisks and a decreasing flow velocity as demonstrated in figure 2. Whereas the H_2O_2 yield is experimentally determined by usage of a second (collector) electrode located in the second compartment of the dual thin-layer flow cell, the relative amount of the desorbed reaction intermediate *B* in the model was determined at the outlet.

Furthermore, we see that the variation of $c_{\mathrm{cat}}^{\mathrm{eff}}$ on a single catalytically active area in the case $L_{\mathrm{cat}} = 64$ yields a result which is very close to that of the variation of the number of small catalytically active areas with fixed $c_{\mathrm{cat}}^{\mathrm{eff}}$ and length $l_{\mathrm{act}} = 1$, provided, the total amount of catalyst N_{cat} is the same.

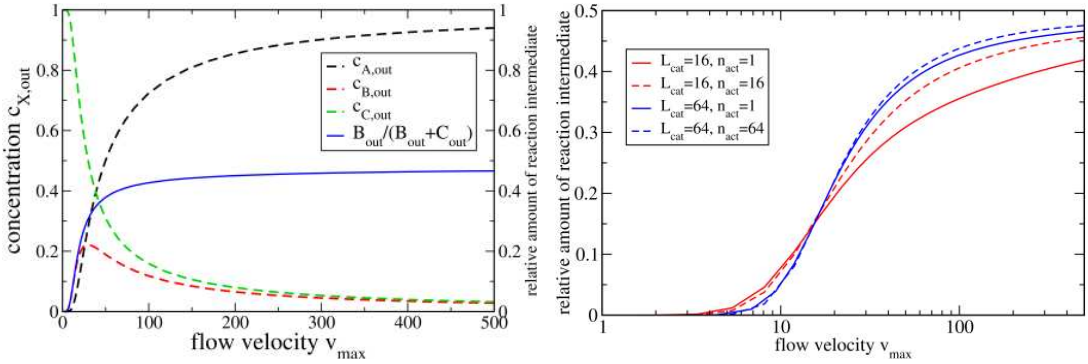

Figure 6: Left: Species concentration and relative amount of reaction intermediates at the outlet depending on the inflow velocity v_{max}. Right: influence of the distribution of the catalyst. Solid lines correspond to one large single catalytically active area; Dashed lines correspond to separate catalytically active areas with the same overall amount of catalyst.

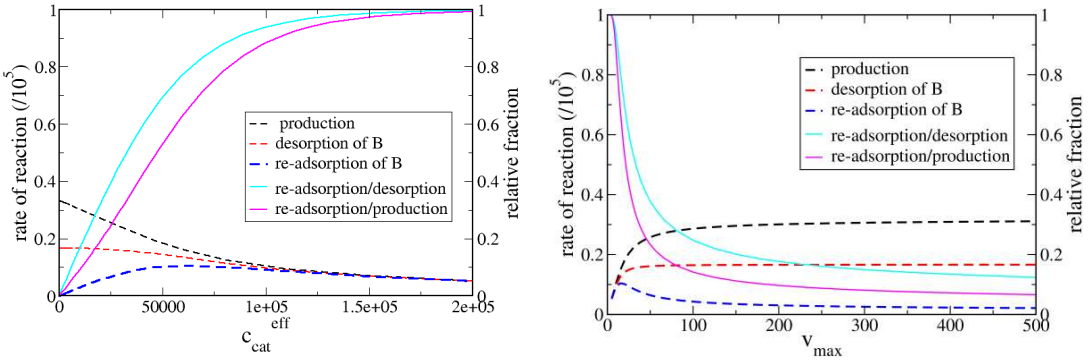

Figure 7: Dependency of rate of production, desorption and re-adsorption of species B and their relative fraction on the amount of catalyst sites per unit volume (left figure) and flow velocity (right figure).

3.3 Variation of the flow velocity

A higher flow velocity moves the desorbed species faster to the outlet. This results in a greater relative amount of reaction intermediates $B_{\mathrm{out}}/(B_{\mathrm{out}} + C_{\mathrm{out}})$ (cf. Figure 6) in good qualitative agreement with experimental findings as shown in Figure 2 and ref. [7]

3.4 The rate of production and re-adsorption

The reaction terms of θ_A, θ_B, θ_C, $c_A\theta_f$, $c_B\theta_f$ and $c_C\theta_f$ can be integrated along the catalyst layer numerically. For stationary state, it was obtained from (9)-(11) that $\theta_A = c_A\theta_f$, $\theta_B = \theta_C$, for the parameters described above. Actually, the integration of $k_{AB}^{+}\theta_A$, $k_B^{-}\theta_B$, $\hat{k}_B^{+}c_B\theta_f$ along the catalyst layer

gives the rates for production, desorption and re-adsorption of species B, which are proportional to the integration of θ_A, θ_B and $c_B\theta_f$. Their dependency on the amount of catalyst site per unit volume and the flow velocity are show in Figure 7.

4 Asymptotic estimates

The surface reaction can be analyzed in laminar boundary layer flows for a continuous electrode according to a method used in [17]. At the electrode surface, according to [18] the concentration field c_X fulfilling (7) in the velocity field with $\vec{v} \cdot \vec{n} = 0$ satisfies the integral equation

$$D_X \partial_n c_X(x,0) \;=\; I[c_X'] \;= D_X \left(\frac{1}{9\mu D_X}\right)^{\frac{1}{3}} \frac{(\tau(x))^{\frac{1}{2}}}{\left(\frac{1}{3}\right)!} \int_0^x \left(\int_{x_1}^x (\tau(z))^{\frac{1}{2}} dz\right)^{-\frac{1}{3}} \partial_{x_1} c_X(x_{1,0}) dx_1 \tag{12}$$

$$c_X(0,0) \;= c_{X0} \tag{13}$$

Here, $\tau(x)$ is the wall shear rate, $\mu = 1$ is the dynamic viscosity.

For Hagen-Poiseuille flow, in the large velocity asymptotic regime, the wall shear rate is

$$\tau = \mu \frac{6\bar{v}}{h_{\text{cell}}} = \mu \frac{4v_{\max}}{h_{\text{cell}}}$$

and the integral (12) becomes

$$I[c_X'] = -\int_0^z \frac{c_X'(z_1)dz_1}{(z^3 - z_1^3)^{\frac{1}{3}}}, c_X(0) = c_{X0},$$

with $z = \left(\frac{1}{3}\right)! \, \frac{1}{D} \left(\frac{9D\, h_{\text{cell}}}{4v_{\max}}\right)^{\frac{1}{3}} x^{\frac{1}{3}}$.

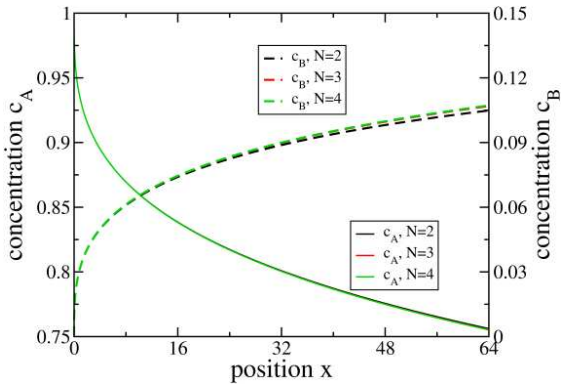

Figure 8: Convergence of the asymptotic solution for $v_{\max} = 100$ and different truncation lengths of the series ansatz.

It is possible to use (9)-(11) in order to exclude the surface coverages from the reaction terms under the assumption that the small reaction constants (cf. Table 1) k_A^-, k_{AB}^-, k_{BC}^- and $\hat{k}_C^+$ are set to zero:

$$\theta_A \;=\; \frac{c_A \hat{k}_A^+ (k_{BC}^+ + k_B^-) k_C^-}{k_4 c_A + k_5 c_B + k_6}$$

$$\theta_B = \frac{c_A k_{AB}^+ \hat{k}_A^+ k_C^- + c_B k_{AB}^+ \hat{k}_B^+ k_C^-}{k_4 c_A + k_5 c_B + k_6}$$
$$\theta_C = \frac{c_A k_{AB}^+ \hat{k}_A^+ k_{BC}^+ + c_B k_{AB}^+ k_{BC}^+ \hat{k}_B^+}{k_4 c_A + k_5 c_B + k_6}$$
$$\theta_f = \frac{k_{AB}^+ (k_{BC}^+ + k_B^-) k_C^-}{k_4 c_A + k_5 c_B + k_6}$$

For brevity, here and in the next equations we used c_X instead of $c_X(x,0)$. In that case, the reaction rates can be expressed as

$$r_A = \frac{(k_1' + k_2') c_A}{k_4 c_A + k_5 c_B + k_6}$$
$$r_B = \frac{-k_1' c_A + k_3' c_B}{k_4 c_A + k_5 c_B + k_6}$$
$$r_C = \frac{-k_2' c_A - k_3' c_B}{k_4 c_A + k_5 c_B + k_6}$$

with $k_1' = k_{AB}^+ \hat{k}_A^+ k_B^- k_C^-$, $k_2' = k_{AB}^+ k_{BC}^+ \hat{k}_A^+ k_C^-$, $k_3' = k_{AB}^+ k_{BC}^+ \hat{k}_B^+ k_C^-$, $k_4 = \hat{k}_A^+ (k_{AB}^+ (k_{BC}^+ + k_C^-) + (k_{BC}^+ + k_B^-) k_C^-)$, $k_5 = k_{AB}^+ \hat{k}_A^+ (k_{BC}^+ + k_C^-)$, $k_6 = k_{AB}^+ (k_{BC}^+ + k_B^-) k_C^-$ and the reaction term in (8)

$$R_A = c_{\text{cat}} r_A = \frac{(k_1 + k_2) c_A}{k_4 c_A + k_5 c_B + k_6}$$
$$R_B = c_{\text{cat}} r_B = \frac{-k_1 c_A + k_3 c_B}{k_4 c_A + k_5 c_B + k_6}$$
$$R_C = c_{\text{cat}} r_C = \frac{-k_2 c_A - k_3 c_B}{k_4 c_A + k_5 c_B + k_6}$$

with $k_1 = k_1' c_{\text{cat}}$, $k_2 = k_2' c_{\text{cat}}$, $k_3 = k_3' c_{\text{cat}}$.

As a result, we obtain a coupled system of functional equations

$$R_X(c_A, c_B, c_C) = I[c_X'] \qquad (X = A, B, C) \tag{14}$$
$$c_A(0,0) = 1 \tag{15}$$
$$c_B(0,0) = 0 \tag{16}$$
$$c_C(0,0) = 0. \tag{17}$$

Using the ansatz

$$c_A = a_0 + \sum_{n=1}^{\infty} (-1)^n a_n z^n, \qquad c_B = b_0 + \sum_{n=1}^{\infty} (-1)^n b_n z^n, \qquad c_A = c_0 + \sum_{n=1}^{\infty} (-1)^n c_n z^n,$$

we develop a series solution of this system. Using Mathematica [19], we gather the coefficients of z^i in (14)-(17) and thus for every i obtain a linear system of equations in the coefficients a_i, b_i, c_i. Mathematica as well allows to obtain the corresponding solutions. Let $g_n = \frac{3\left(\frac{n}{3}-\frac{1}{3}\right)!}{n\left(\frac{n}{3}-1\right)!\left(-\frac{1}{3}\right)!}$.

We obtain for $i = 0$:

$$a_0 = 1 = c_A(0,0)$$
$$b_0 = 0$$
$$c_0 = 0$$

for $i = 1$:

$$a_1 = \frac{a_0 g_1 (k_1 + k_2)}{a_0 k_4 + k_6}$$

$$b_1 = -\frac{a_0 g_1 k_1}{a_0 k_4 + k_6}$$
$$c_1 = -\frac{a_0 g_1 k_2}{a_0 k_4 + k_6}$$

for $i = 2$:

$$a_2 = \frac{a_0 g_1 g_2 (k_1 + k_2)(a_0\, k_2 k_5 + (k_1 + k_2) k_6)}{(a_0 k_4 + k_6)^3}$$
$$b_2 = -\frac{a_0 g_1 g_2 (a_0 k_2 (k_3 k_4 + k_1 k_5) + (k_1^2 + k_1 k_2 + k_2 k_3) k_6)}{(a_0 k_4 + k_6)^3}$$
$$c_2 = -\frac{a_0 g_1 g_2 k_2 (a_0 (-k_3 k_4 + k_2 k_5) + (k_1 + k_2 - k_3) k_6)}{(a_0 k_4 + k_6)^3}$$

For the sake of brevity, we omit the expressions for larger values of i. The surface concentrations c_A, c_B, c_C at the catalytic surface are obtained for $N = 2, 3, 4$, and the solution converges sufficiently already for $N = 4$ (Figure 8). We choose $N = 12$ in order to obtain the calculation results discussed in the sequel.

The above estimate gives the solution on the catalyst surface. The integration of reaction rates along the catalyst surface gives the amount of consumed species A and the amount of released B and C, which are related to the concentration at the outlet. These data allow to compare the asymptotic solution to the numerical solution.

5 Results of asymptotic estimates in comparison to the numerical approach

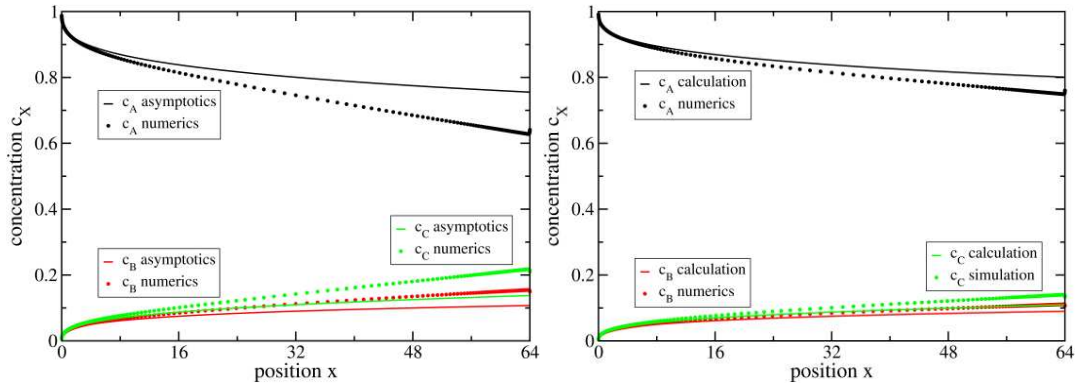

Figure 9: Large velocity asymptotics and numerical results for $c_{\text{cat}}^{\text{eff}} = 10^5$, $L_{\text{cat}} = 64$, $v_{\max} = 100$ (left figure) and $v_{\max} = 200$ (right figure).

The asymptotic solution is compared with the numerical simulation results in Figure 9. For $v_{\max} = 100$, numerical and asymptotic solutions differ quite substantially at larger distance from the electrode edge. This situation improves significantly already for $v_{\max} = 200$.

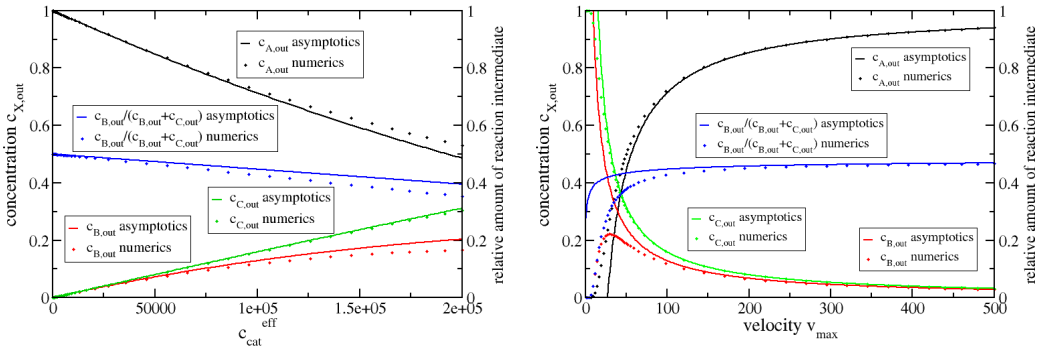

Figure 10: Dependency of the species concentration and the relative amount of reaction intermediates at the outlet on the amount of catalyst sites per unit volume and flow velocity for $L_{\mathrm{cat}} = 64$. Left figure: $v_{\max} = 100$, right figure: $c_{\mathrm{cat}}^{\mathrm{eff}} = 10^5$.

In Figure 10 one observes that the results of the asymptotic approach follow the same trend as the results of the numerical simulations. The relative amount of reaction intermediates decreases with increasing catalyst loading. Due to the relatively large velocity values needed to enter the region of validity of the asymptotic approach, also for higher catalyst loadings, this relative amount still remains significant. At the same time, the relative amount of reaction intermediates increases with increasing velocity. One further observes that with increasing velocity values, the agreement of the results of both approaches increases. This allows to cross-verify the results obtained by both approaches. In particular this result underlines that for the numerical simulation, grid adaptation and alignment at the electrode boundary have been performed with sufficient care.

6 Conclusions and outlook

We have introduced a model describing a multistep consecutive electrocatalytic reaction, which includes desorption, re-adsorption and further reaction of a reactive reaction intermediate, in a rectangular flow cell at given temperature and potential. Starting from the Langmuir model for adsorption and desorption, a mathematical model of this reaction has been developed, which couples convective and diffusive transport with the reaction itself. In order to obtain approximate solutions of the mathematical model, a numerical approach based on the finite volume method, as well as large velocity asymptotics have been developed.

Both approaches can be applied to describe the reaction behaviour of a single catalytically active area, and show similar results. Namely, the relative amount of reaction intermediates in the overall reaction products measured at the outlet of the flow cell is found to decrease with increasing catalyst loading and to increase with increasing velocity. A similar behavior was previously observed experimentally.

With proper precautions taken concerning mesh refinement in the boundary layer and at catalyst edges, the numerical approach is more general than the asymptotic approach and can be applied to an electrode consisting of a number of small catalyst particles. With increasing number of catalytically active areas (or increasing catalyst loading), we find a decrease of the relative amount of reaction intermediates. For an increasing number of catalytically active areas, the numerical results suggest that the solution converges to that of a single catalytically active area with the same amount of catalyst.

The good qualitative agreement of these findings and the experimental results suggests that a coupled macroscopic transport-reaction model, which includes a desorption – re-adsorption equilibrium of the reaction intermediate, represents a reasonable description of the mechanistic scheme proposed in the earlier studies [6,7].

In a coarse approximation, one can assume that an increase of temperature behaves like an increase of c_{cat} if one assumes that the Arrhenius law is included into the definition of the reaction constants. Under this assumption, the model can be easily extended to understand not only experimental results obtained at constant temperature, but also to interpret the influence of temperature for a fixed amount of catalyst.

Subsequent research will focus on a generalization of this model, taking into account possible temperature effects via the Arrhenius equation for reaction rates and diffusion coefficients and potential effects via the Butler Volmer relation.

References

[1] C. H. Hamann, A. Hamnett, and W. Vielstich. Electrochemistry. WILEY-VCH, Weinheim, 1998.

[2] M. R. Tarasevich, A. Sadkowski, and E. Yeager. Oxygen electrochemistry. In B.E. Conway, J. O'M. Bockris, E. Yeager, S.U. M. Khan, and R.E. White, editors, Comprehensive Treatise of Electrochemistry, pages 354-359. Plenum Press, NY and London, 1983.

[3] P.S. Kauranen, E. Skou, and J. Munk. Kinetics of methanol oxidation on carbon-supported Pt and Pt + Ru catalysts. J. Electroanalyt. Chem., 404:1-13, 1996.

[4] Hamnett. Mechanism and electrocatalysis in the direct methanol fuel cell. Catalysis Today, 38:445-458, 1997.

[5] J. Divisek, J. Fuhrmann, K. Gärtner, and R. Jung. Performance modeling of a direct methanol fuel cell. J. Electrochem. Soc., 150:A811-A825, 2003.

[6] A. Schneider, L. Colmenares, Y. E. Seidel, Z. Jusys, B. Wickman, B. Kasemo, and R. J. Behm. Transport effects in the oxygen reduction reaction on nanostructured, planar glassy carbon supported Pt/GC model electrodes. Phys. Chem. Chem. Phys., 10:1931-1943, 2008.

[7] Y. E. Seidel, A. Schneider, Z. Jusys, B. Wickman, B. Kasemo, and R. J. Behm. Mesoscopic mass transport effects in electrocatalytic processes. Faraday Discuss., 140:167 - 184, 2008.

[8] H. Fredriksson, Y. Alaverdyan, A. Dmitriev, C. Langhammer, D.S. Sutherland, M. Zäch, B. Kasemo. Hole-Mask Colloidal Lithography. Adv. Mat. 19:4279-4302, 2007.

[9] Z. Jusys, J. Kaiser, R.J. Behm. Nanostructured platinum-on-carbon model electrocatalysts prepared by colloidal lithography. Electrochimica Acta 49:1297-1305, 2004.

[10] R.W. Lindström, Y.E. Seidel, Z. Jusys, M. Gustavsson, B. Wickman, B. Kasemo and R.J. Behm, Electrocatalysis and transport effects on nanostructured Pt/GC electrodes. J. Electroanal. Chem. 644:90-102, 2010.

[11] Y.E. Seidel, A. Schneider, Z. Jusys, B. Wickmann, B. Kasemo, R.J. Behm. Transport effects in the electrooxidation of methanol studied on nanostructured Pt/glassy carbon electrodes. Langmuir, 26:3569-3578, 2010.

[12] Z. Jusys and R.J. Behm. Methanol, formaldehyde and formic acid adsorption / oxidation on carbon supported Pt nanoparticle fuel cell catalyst: A comparative quantitative DEMS study. In M.T.M. Koper, editor, Fuel Cell Catalysis: A Surface Science Approach, pages 411-464. Wiley, 2009. ISBN: 978-0-470-13116-9.

[13] Y. Liu, R. He, Q. Zhang, and S. Chen, Theory of Electrochemistry for Nanometer-Sized Disk Electrodes. J. Phys. Chem. C, 114:10812–10822, 2010.

[14] L. Wang, U. Stimming, M. Eikerling: Kinetic Model of Hydrogen Evolution at an Array of Au-Supported Catalyst Nanoparticles. Electrocatalysis 1:60-71, 2010.

[15] J. Fuhrmann, H. Zhao, E. Holzbecher, H. Langmach, M. Chojak, R. Halseid, Z. Jusys, and R. Behm. Experimental and numerical model study of the limiting current in a channel flow cell with a circular electrode. Phys. Chem. Chem. Phys., 10:3784 - 3795, 2008.

[16] J. Fuhrmann and H. Langmach. Stability and existence of solutions of time-implicit finite volume schemes for viscous nonlinear conservation laws. Appl. Numer. Math., 37:201-230, 2001.

[17] P. L. Chambre and A. Acrivos. On chemical surface reactions in laminar boundary layer flows. J. Appl. Phys., 27:1322-1328, 1956.

[18] M. J. Lighthill. Contribution to the theory of heat transfer through a laminar boundary layer. Proc. R. Soc. Lond. A, 202:359-377, 1950.

[19] Mathematica 7.0. Wolfram Research Inc., 2009.